VNU Journal of Science: Natural Sciences and Technology
Journal homepage: https://js.vnu.edu.vn/NST

Original Article

Design and Study on Square Lattice-Based Photonic Crystal Fiber with CCl_4 Infiltration under Different Air Holes in the Cladding

Hoang Trong Duc[1], Le Tran Bao Tran[2], Tran Ngoc Thao[2], Chu Van Lanh[2], Nguyen Thi Thuy[1,*]

[1]*University of Education, Hue University, 34 Le Loi, Hue, Vietnam*
[2]*Vinh University, 182 Le Duan, Vinh, Vietnam*

Received 09th August 2023
Revised 19th June 2024; Accepted 26th June 2024

Abstract: In this paper, a new study is made on carbon tetrachloride (CCl_4) infiltrated-photonic crystal fiber (PCF) with the difference between circular air-hole in the innermost layer and others in the square lattice to improve the optical properties. Based on numerical investigation of parameters such as dispersion, effective mode area, nonlinear coefficient, and confinement loss, we obtain a variety of dispersion including all-normal and anomalous dispersion, which is as small as 0.799 ps/nm.km at 1300 nm the pump wavelength. At the same time, the highest value of nonlinear coefficient 458.718 $W^{-1}.km^{-1}$ has been obtained, corresponding to the smallest value of 1.933 μm^2 of the effective mode area at 1550 nm of fiber Λ = 1.0 µm, d_1/Λ = 0.8. We propose two optimal structures for directing in practical applications with supercontinuum generation (SC) in the short-wave infrared wavelength range.

Keywords: Photonic crystal fiber (PCF), square lattice, high nonlinearity coefficient, small effective mode area, low confinement loss, supercontinuum generation.

*Corresponding author.
Email address: ntthuy@hueuni.edu.vn

https://doi.org/10.25073/2588-1140/vnunst.5476

1. Introduction

Published in the 90s, the photonic crystal fiber is an interesting topic attracting the interest of optical research groups around the world due to its excellent propagation properties [1]. Among them, dispersion in PCF has many advantages over conventional optical fibers because the periodic man-made coating consists of micrometer-sized air holes that allow flexible adjustment of dispersion curves [2]. This property will be useful in practical applications such as dispersion compensation, nonlinear optics, optical communication, etc. [3]. Besides, PCFs are also very attractive for the study of nonlinear effects, as they can be flexibly designed to have small effective areas, increase the nonlinear effects, and generate broad supercontinuum (SC) spectra. Compact, coherent, high-power, single-mode broadband optical sources are the target of researchers in various fields of application such as spectroscopy [4, 5], fluorescence microscopy [6], optical coherence tomography [7], optical telecommunication systems [8], biomedical imaging [9], gas sensing [10], frequency comb metrology [11].

In recent years, a lot of research interest has focused on generating SC using PCF for its dispersion optimization. However, it is difficult to control dispersion and low confinement loss over a wide range of wavelengths if conventional PCFs (solid-core silica-based PCFs or with the same air hole diameters) are used. Therefore, two of the many noticed ways to improve the dispersion of PCF are as follows:

First, it is possible to fill the air holes or hollow cores of PCFs, either completely or selectively, with high nonlinearity liquids. Some liquid-infiltrated PCFs such as C_6H_6, $C_6H_5NO_2$, $CHCl_3$, C_7H_8, CS_2, C_2Cl_4, and CCl_4 [12-22] are highly effective in SC generation.

Second, it is possible to select the geometry of the lattice (circular, hexagonal, elliptical,...) and change the air hole diameters in the cladding or the lattice constant. Even rings in the periodic array can be designed differently because the periodicity in the cladding is not necessary to confine the guiding light to the core region. Many publications [17, 19, 22, 23] have also achieved flat dispersion, small, and high nonlinearity as expected.

In this work, we combine both approaches in the design of our PCFs. CCl_4 was chosen because of its nonlinear refractive index of 5 times that of silica and low toxicity [24]. The difference between the air hole diameter d_1 in the first layer near the core and d_2 of the other layers is noted in the design. We chose the square lattice because of its high symmetry, which strongly confines light in the core of the PCF, i.e. enhances the fiber nonlinearities. Furthermore, square lattice PCF can be used in integrated optical devices with rectangular or square cross-sections. With such a design, we have achieved flat dispersion including all-normal and anomalous dispersion, small dispersion value, high nonlinear coefficient, and low confinement loss in comparison with some previous publications about CCl_4-filled PCF. The outstanding advantages make these PCFs well-suited to SC generation applications for all-fiber laser systems.

2. Numerical Modeling of the CCl_4-core PCFs

The square lattice structure of eight air-hole layers is periodically arranged in the cladding surrounding the CCl_4-infiltrated hollow core of PCF. The geometric cross-section of the PCF is shown in Figure 1a. The substrate of PCF is fused silica, and the hollow core is filled with CCl_4 causing the difference in refractive index between the core and the cladding.

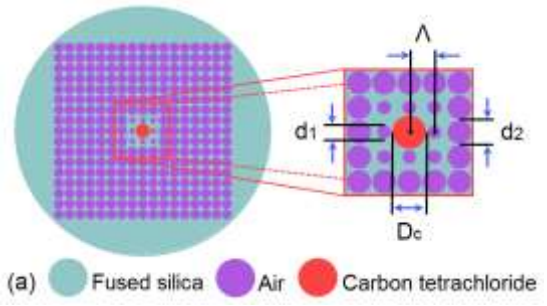

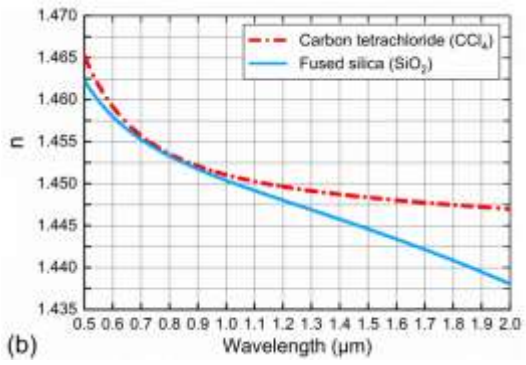

Figure 1. Cross-section view of geometric structure (a), and the real parts of the refractive index n of CCl_4 and SiO_2 (b).

We denote d_1 and d_2 as the air hole diameters of the innermost layer and the other layers, respectively, the lattice constant Λ is the distance from the center of the core to the center of the air hole as well as between air holes to each other. The variation of filling factor d_1/Λ from 0.3 to 0.8 with a step of 0.5 became the design parameter to control the dispersion and nonlinear properties of PCF, and the value of d_2/Λ was kept constant at 0.95 to reduce the confinement loss to the lowest possible value. The large core diameter is determined by the formula $D_c = 2\Lambda - 1.1d_1$ with Λ = 1.0, 1.5, 1.8, and 2.0 μm. Numerical simulations were performed based on solving Maxwell's electromagnetic wave propagation equations by full-vector finite-difference eigenmode (FDE) method using Lumerical Mode Solutions (LMS) software. The finite-difference algorithm is the current method used for meshing the waveguide geometry and can accommodate arbitrary waveguide structure, allowing no reflection at the edge and minimizing loss.

The real parts of the effective refractive index n of carbon tetrachloride and fused silica against the wavelength are displayed in Figure 1b. Interestingly, the linear refractive index of carbon tetrachloride is similar to that of fused silica in the shorter wavelength range and greater than that of fused silica in the longer wavelength region. The dependence of the effective refractive index of fused silica and carbon tetrachloride on the wavelength is described by the Sellmeier equation [25] and Cauchy [26] as follows:

$$n^2_{SiO_2}(\lambda) = 1 + \frac{0.6961663\lambda^2}{\lambda^2 - (0.0684043)^2} + \frac{0.4079426\lambda^2}{\lambda^2 - (0.1162414)^2} + \frac{0.8974794\lambda^2}{\lambda^2 - (9.896161)^2} \quad (1)$$

$$n^2_{CCl_4}(\lambda) = 2.085608282 + 0.00053373\lambda^2 + 0.012201206\lambda^{-2} + 0.000056451\lambda^{-4} + 0.000048106\lambda^{-6} \quad (2)$$

where λ is the excitation wavelength in micrometers, and $n(\lambda)$ is the wavelength-dependent linear refractive index of materials.

Dispersion is a key parameter that determines the characteristics of the SC spectrum because it contributes to the generation of new frequencies when ultrashort pulses propagate in PCFs. Equation (3) [27] below allows to calculate the dispersion numerically:

$$D = -\frac{\lambda}{c}\frac{d^2\,\mathrm{Re}[n_{eff}]}{d\lambda^2} \quad (3)$$

where c and n_{eff} are the speed of light in a vacuum and the effective refractive index of the PCF respectively.

$$n_{eff} = \frac{\beta}{k_0} = \frac{\beta}{2\pi/\lambda} \quad (4)$$

with β as the propagation constant [27], and λ is the wavelength.

As light propagates in PCF, due to its high intensity, it interacts with the physical medium through nonlinear effects characterized by parameters such as effective mode area, nonlinear coefficient, and confinement loss. The degree of limitation of the electromagnetic field in the core of the PCF is expressed as the effective mode area, which depends on the amplitude of the transverse electric field E propagating inside the PCF. This parameter can be determined according to the following formula [28]:

$$A_{\text{eff}} = \frac{\left(\int_{-\infty}^{\infty} \int_{-\infty}^{\infty} |E|^2 \, dxdy \right)^2}{\int_{-\infty}^{\infty} \int_{-\infty}^{\infty} |E|^4 \, dxdy} \quad (5)$$

The frequency-dependent nonlinear coefficient [27] is inversely proportional to the effective mode area, which is related to the linear refractive index and the nonlinear refractive index of the fundamental mode as given below:

$$\gamma(\lambda) = 2\pi \frac{n_2}{\lambda A_{\text{eff}}} \quad (6)$$

The confinement loss is calculated through formula (7) [29], manifesting the relationship between the wavelength and the imaginary part of the effective refractive index. This is a necessary parameter in PCF design because it represents the leakage of the modes.

$$L_c = 8.686 \frac{2\pi}{\lambda} \text{Im}[n_{\text{eff}}(\lambda)] \quad (7)$$

3. Result and Discussion

For the fundamental mode, the curves of the effective refractive index (Re[n_{eff}]) are similar in shape for all cases of d_1/Λ and Λ, shown in Figure 2. The leakage of long wavelengths in the cladding is more than that of short wavelengths resulting in Re[n_{eff}] decreasing with increasing wavelength. For each instance of Λ, Re[n_{eff}] decreases as d_1/Λ increases over the whole investigated wavelength range. In contrast, when d_1/Λ are fixed, Re[n_{eff}] increases with the increase of Λ causing the curves of the effective refractive index to shift upward relative to the horizontal axis. This is due to the larger expansion of the core size and the greater contribution of fused silica to the refractive index of the cladding [16].

The values of Re[n_{eff}] of fibers with different Λ and d_1/Λ at 1.55 µm, which is a common wavelength of commercial lasers, were computed in Table 1. The maximum and minimum values of Re[n_{eff}] were found to be 1.429 and 1.315 for the structures Λ = 2.0 µm, d_1/Λ = 0.3, and Λ = 1.0 µm, d_1/Λ = 0.8, respectively (Figure 2, Table 1).

The role of CCl_4 and ingenious modification of lattice parameters in the design of PCFs have resulted in a diverse dispersion including all-normal and anomalous dispersion depending on the variation of d_1/Λ and Λ. The dependence of dispersion on wavelength and lattice parameters is shown in Figure 3. Some results are obtained as follows:

- For all cases of Λ, the slopes of the dispersion curves increase as the filling factor d_1/Λ increases.

- For the small Λ (Λ = 1.0 µm), anomalous dispersion with one and two zero-dispersion wavelengths (ZDWs) was observed along with the change of the filling factor d_1/Λ. As d_1/Λ gradually increases from 0.3 to 0.45, the ZDWs shift towards a longer wavelength, which is beneficial in choosing a suitable pump wavelength for SC generation. Anomalous dispersion with two ZDWs is found when d_1/Λ is greater than 0.55. A broad SC spectrum can be obtained with the domination of the soliton effect based on this dispersion property.

In particular, we find two all-normal dispersions with d_1/Λ = 0.5 and 0.55, the smooth and highly coherent SC spectra normally produced with the all-normal dispersion regime. Figure 3a shows that, in the wavelength range from 1.2 to 2.0 µm, as the filling factor increases, part of the dispersion curve tends to move down to the zero dispersion line. In case the filling factor is greater than 0.55, the dispersion curves have a parabolic profile and the peaks of these parabolas tend to move above the zero dispersion line. Choosing a filling factor of 0.25 and 0.85 will result in a large dispersion value that is not beneficial for supercontinuum generation orientation. Thus, the diversity in dispersion can help us choose suitable dispersion depending on the purpose of SC generation for further studies.

- When Λ is larger (Λ = 1.5, 1.8, and 2.0 µm), the dispersion develops quite monotonically, the dispersion curves are anomalous with a ZDW over the entire investigated wavelength

range. The values of dispersion increase gradually with the increase of d_1/Λ causing the slopes of the dispersion curves to increase. The newly generated wavelength components in the SC study have the role of such a high dispersion slope. On the other hand, with a lattice constant Λ = 2.0 µm, the dispersion curve tends to move close to the zero dispersion curve if the filling factor is small, but unfortunately, light is not well confined in the core of PCFs when the filling coefficient is less than 0.3 (Figure 4b1). Therefore, the filling factors less than 0.3 and greater than 0.8 are not considered in all simulations.

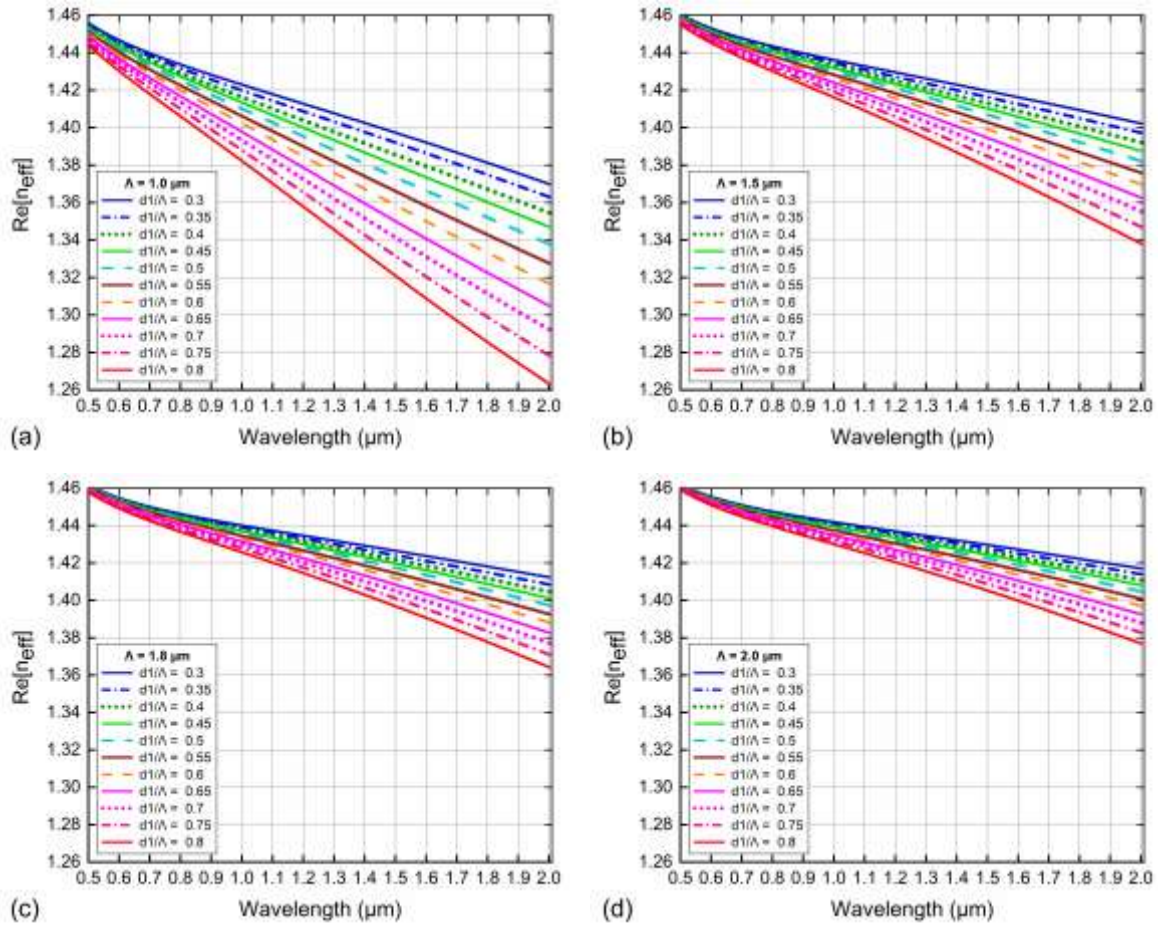

Figure 2. The real part of effective refractive index as a function of wavelength of square-PCFs with various d_1/Λ for (a) Λ = 1.0 µm, (b) Λ = 1.5 µm, (c) Λ = 1.8 µm and (d) Λ = 2.0 µm.

Table 1. The real part of the effective refractive index of square-PCFs with various Λ and d_1/Λ at 1.55 µm wavelength

d_1/Λ	$Re[n_{eff}]$			
	Λ = 1.0 (µm)	Λ = 1.5 (µm)	Λ = 1.8 (µm)	Λ = 2.0 (µm)
0.3	1.395	1.418	1.425	1.429
0.35	1.389	1.414	1.423	1.427
0.4	1.383	1.411	1.42	1.425

0.45	1.377	1.408	1.418	1.423
0.5	1.370	1.405	1.416	1.421
0.55	1.362	1.400	1.412	1.418
0.6	1.354	1.396	1.410	1.416
0.65	1.345	1.392	1.406	1.413
0.7	1.336	1.387	1.402	1.410
0.75	1.326	1.381	1.398	1.406
0.80	1.315	1.375	1.394	1.403

Based on the the above analysis, we introduce two structures including Λ = 1.0 µm, d_1/Λ = 0.55 and Λ = 2.0 µm, d_1/Λ = 0.3 with small and flat dispersion suitable for generation SC. With the first structure, the pump wavelength is chosen as 1.095 µm which is close to the maximum value of the all-normal dispersion curve Λ = 1.0 µm, d_1/Λ = 0.55, the dispersion value at this pump wavelength is quite small of –7.503 ps/nm.km. The second structure has anomalous dispersion with dispersion values as small as 0.799 ps/nm.km at 1.3 µm pump wavelength. These two optimal structures have smaller dispersion than some previous work on hollow-core PCF infiltration to other fluids [15–18, 20–22].

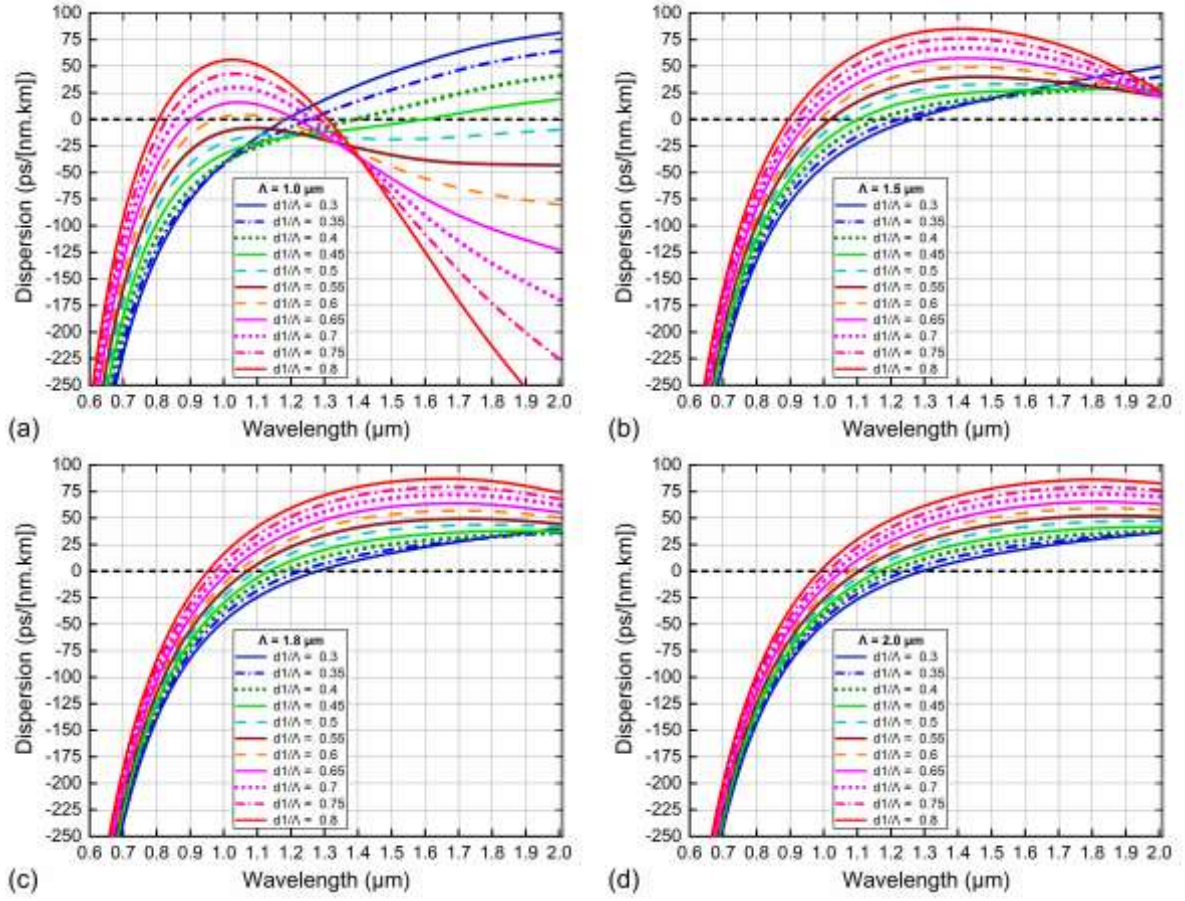

Figure 3. The dispersion as a function of wavelength of square-PCFs with various d_1/Λ for (a) Λ = 1.0 µm, (b) Λ = 1.5 µm, (c) Λ = 1.8 µm and (d) Λ = 2.0 µm.

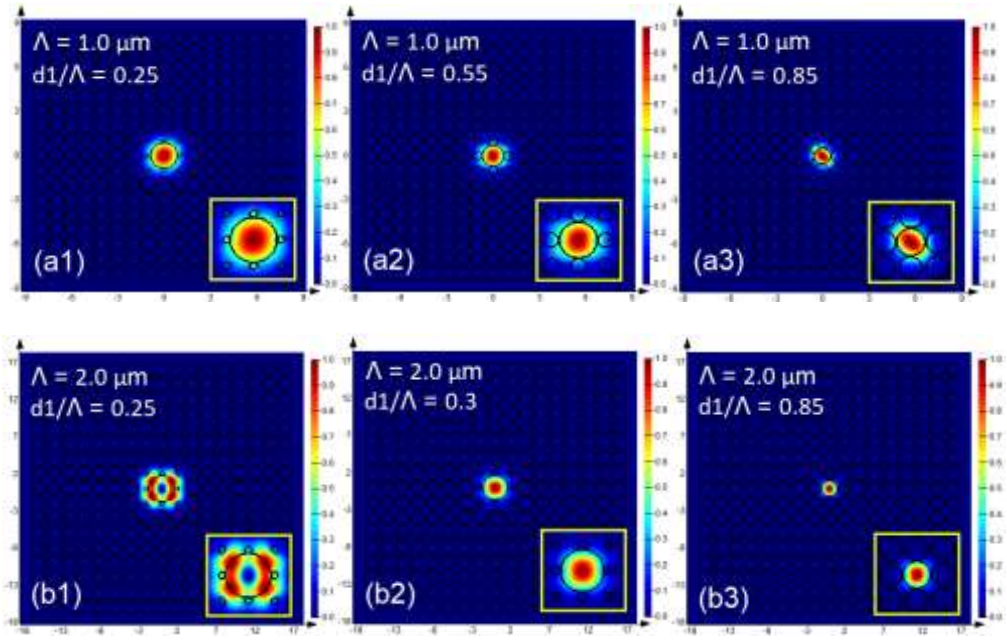

Figure 4. Intensity distribution in square lattice-based PCFs filled with CCl_4 with various d_1/Λ and Λ.

The effective mode area increases with wavelength as illustrated in Figure 5. The square lattice structure with high symmetry is one of the favorable factors for good confinement of light into the core resulting in a small effective mode area for all survey structures. This is one of the outstanding advantages of our research. For each fixed Λ, the increase of the filling factor d_1/Λ reduces the effective mode area.

As Λ varies, although the effective mode area curve shape is similar, its value increases with the increase of Λ. With the same value of d_1/Λ, larger cores reduce light confinement in the core leading to an increased effective mode area.

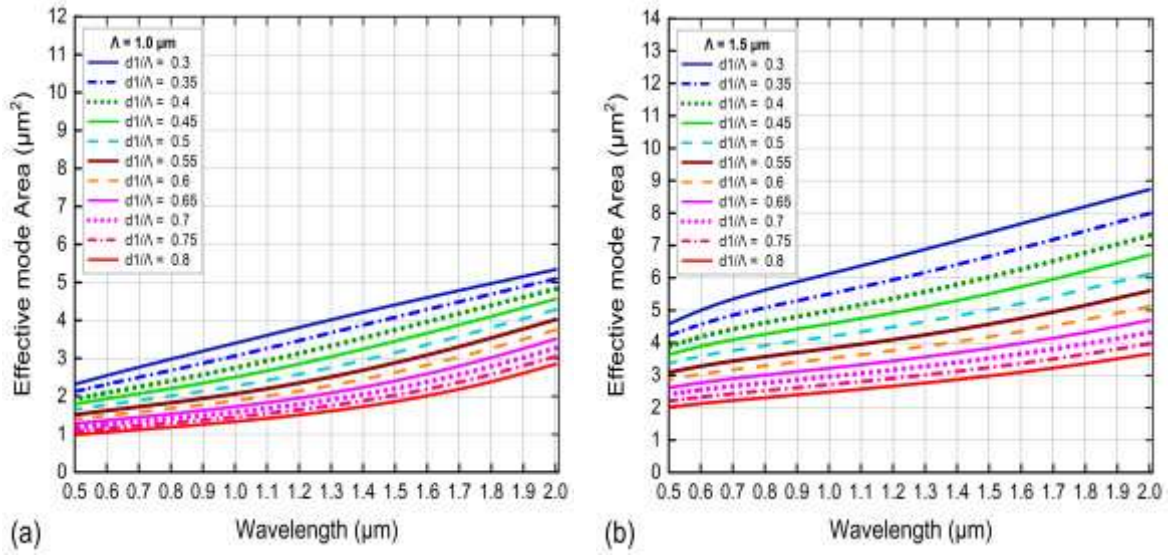

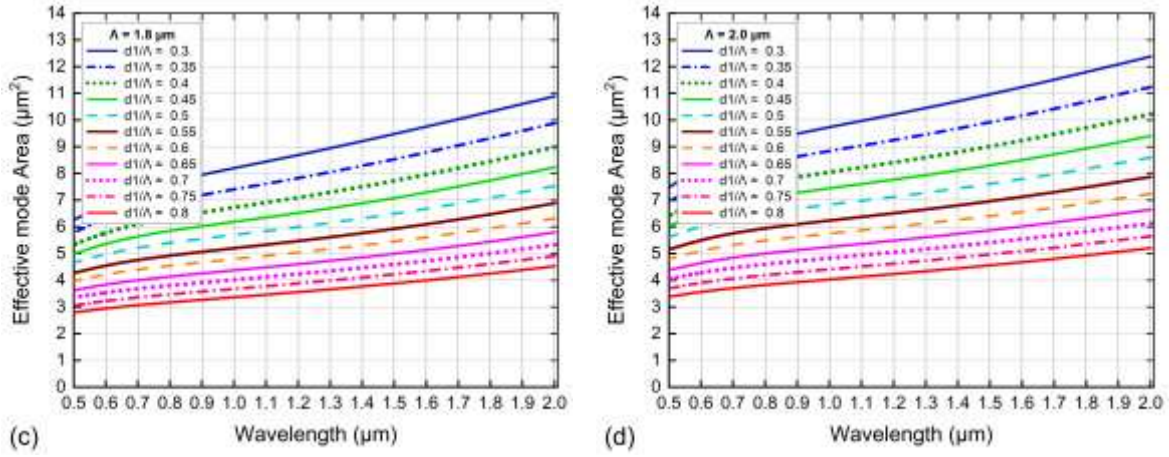

Figure 5. The effective mode area as a function of wavelength of square-PCFs with various d_1/Λ for (a) Λ = 1.0 μm, (b) Λ = 1.5 μm, (c) Λ = 1.8 μm and (d) Λ = 2.0 μm.

The values of the effective mode area according to the variation of Λ and d_1/Λ calculated at a wavelength of 1.55 μm are presented in Table 2. The minimum and maximum values of the effective mode area are 1.933 μm^2 and 11.099 μm^2 correspond to the structures Λ = 1.0 μm, d_1/Λ = 0.8, and Λ = 2.0 μm, d_1/Λ = 0.3, respectively. For the structures with optimal dispersion introduced in the above section (Λ = 1.0 μm, d_1/Λ = 0.55 and Λ = 2.0 μm, d_1/Λ = 0.3), we find a small value of the effective mode area at the pump wavelengths are 2.982 μm^2 and 10.45 μm^2. These values are quite suitable for SC generation and smaller in comparison with previous studies on hollow-core PCF filled by CCl_4 [21, 22].

Table 2. The effective mode area of square-PCFs with various Λ and d_1/Λ at 1.55 μm wavelength

d_1/Λ	A_{eff} (μm^2)			
	Λ = 1.0 μm	Λ = 1.5 μm	Λ = 1.8 μm	Λ = 2.0 μm
0.3	4.506	7.540	9.616	11.099
0.35	4.185	6.792	8.657	10.040
0.4	3.855	6.146	7.842	9.119
0.45	3.555	5.621	7.184	8.403
0.5	3.253	5.113	6.584	7.697
0.55	2.982	4.661	6.012	7.041
0.6	2.724	4.266	5.529	6.482
0.65	2.497	3.906	5.063	5.944
0.7	2.288	3.591	4.659	5.478
0.75	2.101	3.301	4.284	5.031
0.8	1.933	3.036	3.938	4.620

Because the nonlinear coefficient is inversely proportional to the effective mode area, its characteristics are exactly the opposite of the effective mode area (Figure 5). The nonlinear coefficient values are quite high for the two optimal structures (Λ = 1.0 µm, d_1/Λ = 0.55 and Λ = 2.0 µm, d_1/Λ = 0.3) at the pump wavelength: 403.803 ($W^{-1}.km^{-1}$) and 84,728 ($W^{-1}.km^{-1}$).

The relationship between confinement loss and wavelength is exposed in Figure 6. A low confinement loss indicates that the modes are less likely to leak out of the core region of the PCFs. For all cases, confinement loss goes from a high to a low value as d_1/Λ and Λ increase. In the longer wavelength region, the confinement loss is large because low-frequency light is not strongly confined in the core leading to the modes being leaked into the cladding of the PCFs. At wavelength 1.55 µm, we calculate the values of the confinement loss and present them in Table 3. The minimum value of the confinement loss is 21.306 dB/m for fiber Λ = 2.0 µm, d_1/Λ = 0.8. The optimal fibers mentioned above have low confinement losses at the pump wavelength of 15.838 dB/m and 26.487 dB/m, respectively (Λ = 1.0 µm, d_1/Λ = 0.55 and Λ = 2.0 µm, d_1/Λ = 0.3).

Table 3. The confinement loss of square-PCFs with various Λ and d_1/Λ at 1.55 µm wavelength

d_1/Λ	L_c (dB/m)			
	Λ = 1.0 µm	Λ = 1.5 µm	Λ = 1.8 µm	Λ = 2.0 µm
0.30	88.931	64.806	54.978	49.873
0.35	86.790	61.326	51.699	46.821
0.40	83.738	58.175	48.898	44.304
0.45	81.793	56.150	47.100	42.945
0.50	80.102	54.506	45.985	41.859
0.55	77.525	52.509	44.369	40.499
0.60	76.105	51.789	44.033	40.254
0.65	73.966	50.586	43.134	39.497
0.70	73.258	50.758	43.428	39.884
0.75	72.040	50.599	43.529	39.942
0.8	71.957	51.454	44.339	40.786

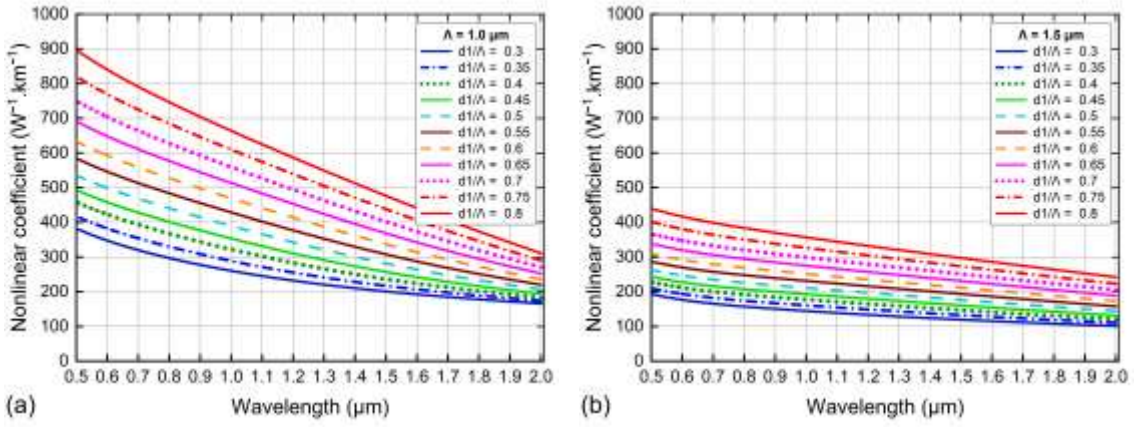

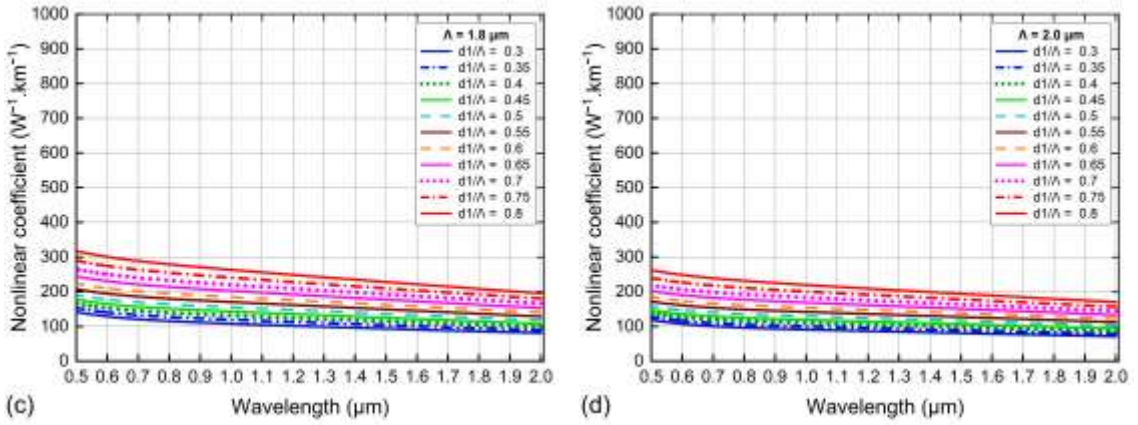

Figure 6. The nonlinear coefficient as a function of wavelength of square-PCFs with various d_1/Λ for (a) Λ = 1.0 μm, (b) Λ = 1.5 μm, (c) Λ = 1.8 μm and (d) Λ = 2.0 μm.

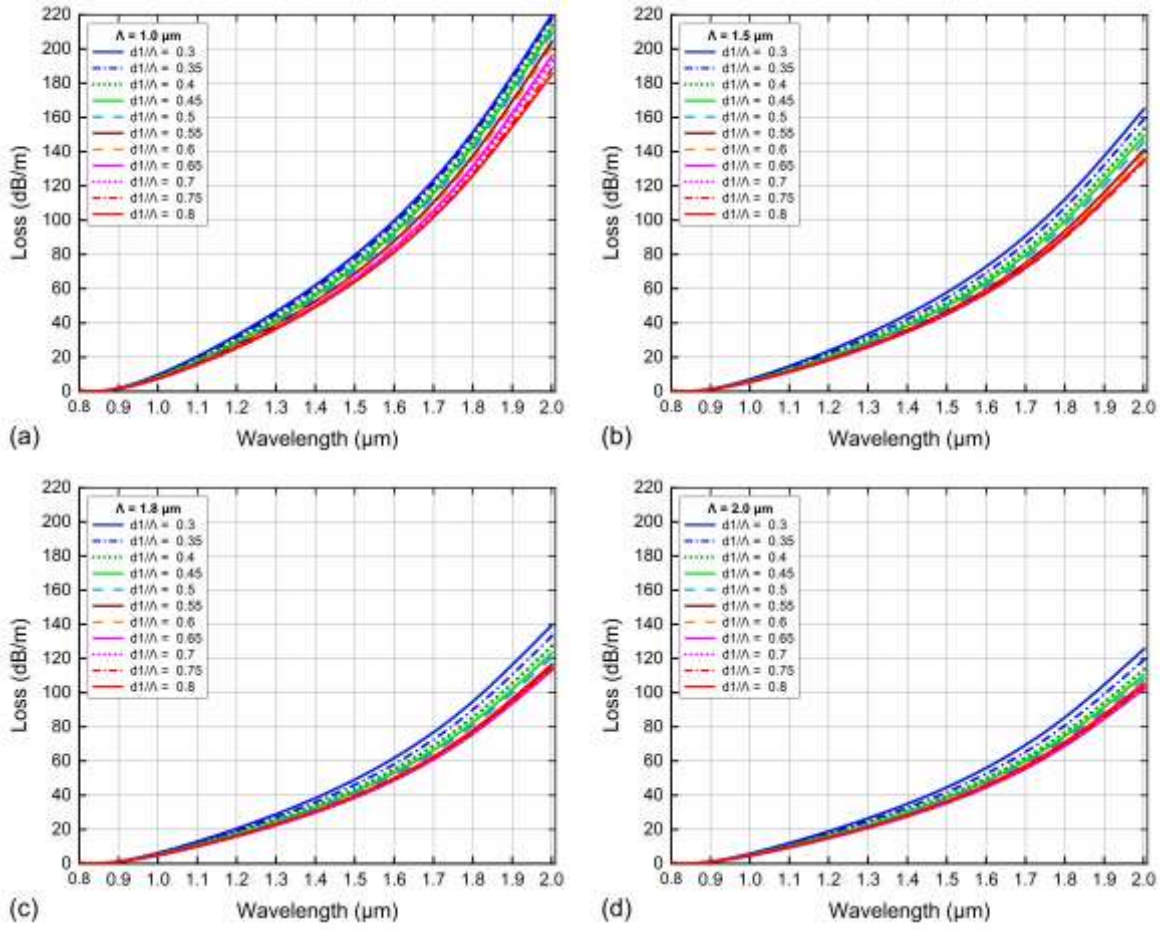

Figure 7. The confinement loss as a function of wavelength of square-PCFs with various d_1/Λ for (a) Λ = 1.0 μm, (b) Λ = 1.5 μm, (c) Λ = 1.8 μm and (d) Λ = 2.0 μm.

The selection of air holes size and core size gives us to achieve low values of confinement loss, the values of L_c at the pump wavelength are 3.904 dB/m and 18.015 dB/m of two fibers Λ = 1.0 µm, d_1/Λ = 0.6 and Λ = 2.0 µm, d_1/Λ = 0.3 respectively. Although the fiber Λ = 2.0 µm, d_1/Λ = 0.3 has a higher confinement loss than the other fiber, it has much lower dispersion. Therefore, this fiber is capable of generating a wide SC spectrum through the soliton effect with input energy as low as nano joules.

4. Conclusion

By cleverly selecting a highly nonlinear liquid-like CCl_4 to fill the hollow core of PCFs and modifying the structural parameters taking into account the recirculation loss of air pores in the mantle (air holes diameter d_1 differs from d_2), we have obtained some outstanding results as follows: Firstly, the achieved dispersion is quite diverse, flat and has a value as small as 0.799 ps/nm.km which is suitable for SC generation. Second, the dispersion and nonlinear characteristics at the pump wavelength of two optimal structures have been analyzed in detail to have a suitable orientation in practical applications. Third, the effective mode area of all the designed PCFs has a small value leading to a large nonlinearity and the maximum value is 458.718 $W^{-1}.km^{-1}$ at the wavelength of commercial lasers of 1.55 µm. Fourth, we get a small value of the confinement loss at wavelength 1.55 µm. These obtained results demonstrate the high applicability of designed PCFs in low-cost all-fiber laser systems.

References

[1] J. C. Knight, Photonic Crystal Fibers, Nature, Vol. 424, 2003, pp. 847-851, https://doi.org/10.1038/nature01940.

[2] M. J. Gander, R. McBride, J. D. C. Jones, D. Mogilevtsev, T. A. Birks, J. C. Knight, P. S. J. Russell, Experimental Measurement of Group Velocity Dispersion in Photonic Crystal Fibre, Electronics Letters, Vol. 35, No. 1, 1999, pp. 63-64, https://doi.org/10.1049/el:19990055.

[3] P. S. Maji, and P. R Chaudhuri, Design of All-Normal Dispersion Based on Multi-material Photonic Crystal Fiber in IR Region for Broadband Supercontinuum Generation, Applied Optics, Vol. 54, No. 13, 2015, pp. 4042-4048, https://doi.org/10.1364/AO.54.004042.

[4] P. Li, K. Shi, Z. Liu, Optical Scattering Spectroscopy by using Tightly Focused Supercontinuum, Optics Express, Vol. 13, No. 12, 2005, pp. 9039-9044, https://doi.org/10.1364/OPEX.13.009039.

[5] K. Shi, P. Li, Z. Liu, Broadband Coherent Anti-Stokes Raman Scattering Spectroscopy in Supercontinuum Optical Trap, Applied Physics Letters, Vol. 90, No. 14, 2007, pp. 141116, https://doi.org/10.1063/1.2720295.

[6] C. Poudel, C. F. Kaminski, Supercontinuum Radiation in Fluorescence Microscopy and Biomedical Imaging Applications, Journal of the Optical Society of America B, Vol. 36, No. 2, 2019, pp. A139-A153, https://doi.org/10.1364/JOSAB.36.00A139.

[7] C. Chen, W. Shi, R. Reyes, V. X. Yang, Buffer-Averaging Super-Continuum Source Based Spectral Domain Optical Coherence Tomography for High Speed Imaging, Biomedical Optics Express, Vol. 9, No. 12, 2018, pp. 6529-6544, https://doi.org/10.1364/BOE.9.006529.

[8] S. Smirnov, J. A. Castanon, T. Ellingham, S. Kobtsev, S. Kukarin, S. Turitsyn, Optical Spectral Broadening and Supercontinuum Generation in Telecom Applications, Optical Fiber Technology, Vol. 12, No. 2, 2006, pp. 122-147, https://doi.org/10.1016/j.yofte.2005.07.004.

[9] N. Nishizawa, H. Kawagoe, M. Yamanaka, M. Matsushima, K. Mori, T. Kawabe, Wavelength Dependence of Ultrahigh-Resolution Optical Coherence Tomography using Supercontinuum for Biomedical Imaging, IEEE IEEE Journal of Selected Topics in Quantum Electronics, Vol. 25, No. 1, 2018, pp. 7101115, https://doi.org/10.1109/JSTQE.2018.2854595.

[10] K. E. Jahromi, Q. Pan, L. Høgstedt, S. M. Friis, A. Khodabakhsh, P. M. Moselund, F. J. Harren, Mid-infrared Supercontinuum-based Upconversion Detection for Trace Gas Sensing, Optics Express, Vol. 27, No. 17, 2019, pp. 24469-24480, https://doi.org/10.1364/OE.27.024469.

[11] J. Yuan, Z. Kang, F. Li, X. Zhang, X. Sang, Q. Wu, B. Yan, K. Wang, X. Zhou, K. Zhong, G. Zhou, C. Yu, C. Lu, H.Y. Tam, and P. K. A. Wai, Mid-infrared Octave-spanning Supercontinuum and Frequency Comb Generation in a Suspended Germanium-membrane Ridge Waveguide, Journal of Lightwave Technology, Vol. 35, No. 14, 2017, pp. 2994-3002, https://doi.org/10.1109/JLT.2017.2703644.

[12] L. C. Van, V. T. Hoang, V. C. Long, K. Borzycki, K. D. Xuan, V. T. Quoc, M. Trippenbach, R. Buczyński, J. Pniewski, Supercontinuum Generation in Benzene-filled Hollow-core Fibers, Optical Engineering, Vol. 60, No. 11, 2021, pp. 116109, http://doi.org/10.1117/1.OE.60.11.116109.

[13] L. C. Van, V. T. Hoang, V. C. Long, K. Borzycki, K. D. Xuan, V. T. Quoc, M. Trippenbach, R. Buczyński, J. Pniewski, Supercontinuum Generation in Photonic Crystal Fibers Infiltrated with Nitrobenzene, Laser Physics, Vol. 30, No. 3, 2020, pp. 035105, https://doi.org/10.1088/1555-6611/ab6f09.

[14] Y. Guo, J. H. Yuan, K. Wang, Generation of Supercontinuum and Frequency Comb in a Nitrobenzene-core Photonic Crystal Fiber with All-normal Dispersion Profile, Optics Communications, Vol. 481, No. 4, 2021, pp. 126555, https://doi.org/10.1016/j.optcom.2020.126555.

[15] L. C. Van, V. T. Hoang, V. C. Long, K. Borzycki, K. D. Xuan, V. T. Quoc, M. Trippenbach, R. Buczyński, and J. Pniewski, Optimization of Optical Properties of Photonic Crystal Fibers Infiltrated with Chloroform for Supercontinuum Generation, Laser Physics, Vol. 29, No. 7, 2019, pp. 075107-075109, https://doi.org/10.1088/1555-6611/ab2115.

[16] L. C. Van, A. Anuszkiewicz, A. Ramaniuk, R. Kasztelanic, K. D. Xuan, V. C. Long, M. Trippenbach, R. Buczyński, Supercontinuum Generation in Photonic Crystal Fibres with Core Filled with Toluene, Journal of Optics, Vol. 19, No. 12, 2017, pp. 125604, https://doi.org/10.1088/2040-8986/aa96bc.

[17] T. N. Thi, D. H. Trong, B. T. L. Tran, T. D. Van, L. C. Van, Optimization of Optical Properties of Toluene-core Photonic Crystal Fibers with Circle Lattice for Supercontinuum Generation, Journal of Optics, 2022, https://doi.org/10.1007/s12596-021-00802-y.

[18] R. Ahmad, M. Komanec, S. Zvanovec, Ultra-wideband Mid-infrared Supercontinuum Generation in Liquid-filled Circular Photonic Crystal Fiber, Journal of Nanophotonics, Vol. 14, No. 2, 2020, pp. 026016, https://doi.org/10.1117/1.JNP.14.026016.

[19] L. C. Van, H. V. Le, N. D. Nguyen, N. V. T. Minh, Q. H. Dinh, V. T. Hoang, T. N. Thi, B. C. Van, Modeling of Lead-bismuth Gallate Glass Ultra-flatted Normal Dispersion Photonic Crystal Fiber Infiltrated with Tetrachloroethylene for High Coherence Mid-infrared Supercontinuum Generation, Laser Physics, Vol. 32, 2022, pp. 055102-12, https://doi.org/10.1088/1555-6611/ac599b.

[20] Q. H. Dinh, J. Pniewski, H. L. Van, A. Ramaniuk, V. C. Long, K. Borzycki, D. X. Khoa, M. Klimczak, R. Buczyński, Optimization of Optical Properties of Photonic Crystal Fibers Infiltrated with Carbon Tetrachloride for Supercontinuum Generation with Subnanojoule Femtosecond Pulses, Applied Optics, Vol. 57, No. 14, 2018, pp. 3738-3746, https://doi:10.1364/ao.57.003738.

[21] V. T. Hoang, R. Kasztelanic, A. Filipkowski, G. Stępniewski, D. Pysz, M. Klimczak, S. Ertman, V. C. Long, T. R. Woliński, M. Trippenbach, K. D. Xuan, M. Śmietana, and R. Buczyński, Supercontinuum Generation in an All-normal Dispersion Large Core Photonic Crystal Fiber Infiltrated with Carbon Tetrachloride, Optical Materials Express, Vol. 9, No. 5, 2019, pp. 2264-2278, https://doi.org/10.1364/OME.9.002264.

[22] V. T. Hoang, R. Kasztelanic, G. Stępniewski, K. D. Xuan, V. C. Long, M. Trippenbach, M. Klimczak, R. Buczyński, J. Pniewski, Femtosecond Supercontinuum Generation around 1560 nm in Hollow-core Photonic Crystal Fibers Filled with Carbon Tetrachloride, Applied Optics, Vol. 59, No. 12, 2020, pp. 3720-3725, https://doi.org/10.1364/AO.385003.

[23] M. Z. Alam, M. I. Tahmid, S. T. Mouna, M. A. Islam, M. S. Alam, Design of a Novel Star Type Photonic Crystal Fiber for Mid-infrared Supercontinuum Generation, Optics Communications, Vol. 500, 2021, pp. 127322, https://doi.org/10.1016/j.optcom.2021.127322.

[24] J. Challenor, Toxicology of Solvents, Rapra Technology Ltd, 2002, ISBN: 1-85957-296-0, https://doi/10.1093/occmed/52.6.363-a.

[25] C. Z. Tan. Determination of Refractive Index of Silica Glass for Infrared Wavelengths by Ir Spectroscopy, Journal of Non-Crystalline Solids, Vol. 223, No. 1-2, 1998, pp. 158-163, https://doi.org/10.1016/s0022-3093(97)00438-9.

[26] K. Moutzouris, M. Papamichael, S. C. Betsis, I. Stavrakas, G. Hloupis, D. Triantis, Refractive, Dispersive and Thermo-optic Properties of Twelve Organic Solvents in the Visible and Near-infrared, Applied Physics B, Vol. 116, No. 3, 2013, pp. 617-622, https://doi.org/10.1007/s00340-013-5744-3.

[27] G. P. Agrawal, Nonlinear Fiber Optics, 5th Edition, Academic Press, Elsevier, 2013, ISBN: 978-0-12-397023-7, https://doi.org/10.1016/C2011-0-00045-5.

[28] K. Saitoh, M. Koshiba, T. Hasegawa, E. Sasaoka, Chromatic Dispersion Control in Photonic Crystal Fibers: Application to Ultra-flattened Dispersion, Optics Express, Vol. 11, No. 8, 2003, pp. 843-852, https://doi.org/10.1364/OE.11.000843.

[29] F. Begum, Y. Namihira, T. Kinjo, S. Kaijage, Supercontinuum Generation in Square Photonic Crystal Fiber with Nearly Zero Ultra-flattened Chromatic Dispersion and Fabrication Tolerance Analysis, Optics Communications, Vol. 284, No. 4, 2011, pp. 965-970, https://doi.org/10.1016/j.optcom.2010.10.029.